Reflection microscope for actinic mask inspection and other progress in soft x-ray laser nano-imaging

C. S. Menoni[1], F. Brizuela[1], S. Carbajo[1], Y. Wang[1], D. Alessi[1], D. H. Martz[1], B. Luther[1], M. C. Marconi[1], J. J. Rocca[1], A. Sakdinawat[2], W. Chao[3], Y. W. Liu[2], E. H. Anderson[3], K. A. Goldberg[3], D. T. Attwood[2], A. V. Vinogradov[4], I. A. Artioukov[4], B. LaFontaine[5]

[1] NSF ERC for Extreme Ultraviolet Science and Technology, and ECE Department, Colorado State University, Fort Collins, USA
[2] NSF ERC for Extreme Ultraviolet Science and Technology, and ECE Department, University of California, Berkeley
[3] NSF ERC for Extreme Ultraviolet Science and Technology, and Center for X-Ray Optics, LBNL, Berkeley, USA
[4] P. N. Lebedev Physical Institute, Moscow, Russia
[5] GLOBALFOUNDRIES, 1050 E. Arques Avenue, Sunnyvale, CA, USA

Abstract. We describe the implementation of a zone plate microscope for at-wavelength characterization of extreme ultraviolet masks. The microscope uses as illumination the 13.2 nm wavelength output from a table-top Ni-like Cd laser. The microscopy allows inspection of EUVL masks under illumination conditions similar to those used in a 4×-demagnification lithographic stepper. High quality EUV images of absorption patterns in EUVL masks have been obtained. Analysis of these images allows characterizing the printability of patterns and defects on the wafer prior to utilization of the mask for production.

1 Introduction

Advances in the development of small laboratory scale soft x-ray (SXR) and extreme ultraviolet (EUV) lasers are driving the implementation of applications, including microscopy, holography, patterning and spectrometry. These techniques exploit the high energy per pulse, short wavelength (high photon energy), to achieve tens of nanometers spatial resolution as is the case of imaging and patterning, and to analyse the chemical composition and reactions of nanoclusters with unprecedented resolution. [1-4]

Several aspects of SXR lasers make them attractive as illumination sources for full field microscopy. The low beam divergence allows for complete

J. Lee et al. (eds.), *X-Ray Lasers 2010,* Springer Proceedings in Physics 136,
DOI 10.1007/978-94-007-1186-0_41,

collection of the SXR light using typical EUV/SXR optics resulting in high throughput efficiency. The narrow spectral bandwidth of the laser output when combined with diffractive optics eliminates chromatic aberrations in the imaging systems. The tuneable degree of coherence allows for a variety of imaging configurations from coherent imaging to imaging under partially coherent light. Furthermore the large number of photons per pulse allows to capture images with a single laser shot thus enabling stop-motion imaging of fast processes due to their short pulse duration of the laser output.

At Colorado State University we have developed full field microscopes that use as illumination the output from SXR lasers based on discharge and laser produced plasma excitation. [1, 5-8]These wavelength-scalable microscopes operate in transmission and reflection configurations to image nanostructures and surfaces with tens of nanometer. Using a very compact microscope illuminated by a SXR laser emitting at 46.9 nm wavelength, we have demonstrated imaging with a near-wavelength spatial resolution of 50 nm, and temporal resolution of 1.2 ns obtained with single laser shot exposure in transmission mode [1]. The same system has been demonstrated in reflection mode with measured spatial resolution better than 200 nm [6]. We have also demonstrated a full-field transmission mode microscope using a SXR laser emitting at either 13.2 nm or 13.9 nm [8]. Using this system, the highest spatial resolution achieved using a SXR/EUV laser based microscope, 38 nm, was obtained with exposure times of 20 seconds and the laser operating at 5 Hz. [8]

In this paper we describe the demonstration of the first compact SXR/EUV laser-based actinic microscope developed specifically to address the evaluation of printability of patterns and defects on extreme ultraviolet lithography (EUVL) masks.

2. Actinic microscopy for Extreme Ultraviolet Mask characterization

The implementation of a reflection microscope at λ=13.2 nm was motivated by the critical needs of EUV lithography (EUVL) to have alternative methods to evaluate the masks used in EUVL steppers. The resonant-reflective nature of these multilayer-coated masks requires that these aerial imaging systems operate at SXR/EUV wavelengths near 13.4 nm.

Actinic (at-wavelength) aerial imaging systems are full-field microscopes that can render information on the printability of patterns and defects prior to wafer printing and are greatly needed for the implementation of EUVL at high-volume manufacturing [9]. Actinic full-field microscopes have been demonstrated using synchrotron illumination and though they have greatly

impacted the development of EUVL masks, they are not practical for manufacturing settings. [10-12]

The table-top aerial EUVL mask characterization microscope described herein combines the output of a table-top 13.2 nm wavelength laser with state-of-the-art diffractive optics to render high quality images of periodic patterns on EUVL masks with acquisition times of less than 90 seconds. From these high quality images we have obtained the line-edge roughness and normalized intensity line slope of EUVL mask. This is significant because, using this table-top microscope, that emulates the imaging conditions of a 4×-demagnification stepper, it is possible to assess the mask quality and printability without the need to test it using an EUVL stepper.

2 Microscope setup

The compact full-field actinic microscope is schematically shown in Fig. 1. The illumination is provided by a table-top, optically pumped, collisional EUV laser that produces a pencil-like output consisting of pulses with a time duration of ~5 ps at a wavelength of 13.2 nm[13]. This laser has been recently operated at repetition rates of up to 2.5 Hz producing an average power of approximately 20 μW at 13.9 nm wavelength using a silver target [14]. To obtain the results reported here, the laser was operated at 1 Hz repetition rate to produce an average power of a several μW in the 13.2 nm line of nickel-like cadmium. The laser produces highly monochromatic ($\Delta\lambda/\lambda<1x10^{-4}$) light pulses with a divergence of 9±0.5 mrad FWHM parallel to the slab target and 10±0.5 mrad in the perpendicular direction. Figure 1 shows schematically the microscope geometry. The laser output is guided to a zone plate condenser that focuses the light onto the EUVL mask. A bright field image of the illuminated region is formed onto a EUV/SXR-sensitive array detector by an off-axis zone plate.

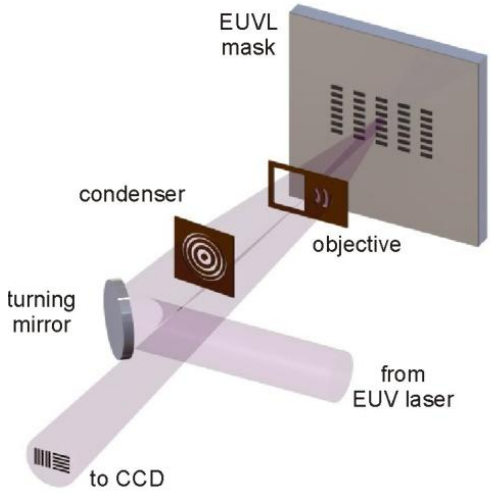

Fig. 1. Schematic of the aerial actinic mask inspection full-field microscope. The system is designed to image the mask with illumination conditions that are similar those of a 0.25 NA, 4×-demagnification EUVL stepper.

The microscope is designed to illuminate the mask as it is done using a 0.25 NA, 4×-demagnification EUVL stepper to correctly evaluate the printability of patterns and defects. This configuration is achieved by selecting the angle of incidence of the illumination onto the mask to be 6 degrees and by tailoring the numerical apertures of the condenser and objective lenses. The condenser zone plate is shown in Fig. 2. The zone plate has a 5 mm diameter, 12000 zones and an outer zone-width of 100 nm, resulting in a numerical aperture (NA) of 0.066 and a focal distance of 38 mm. The diameter of the condenser ensures complete collection of the laser beam.

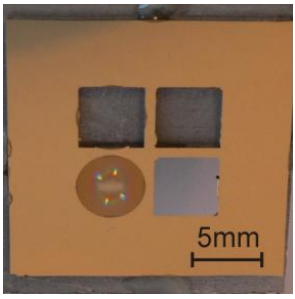

Fig. 2. Photograph of the condenser zone plate. The open window next to the zone plate allows the image formed by the objective to reach the CCD detector.

A scanning electron microscope (SEM) image of the objective zone plate is shown in Fig. 3. The off-axis zone plate was designed from a regular 'parent'

zone plate (dashed line in the figure) with a diameter of 0.33 mm and an outer zone width of 40 nm onto which a smaller pupil is overlapped. The pupil, ~0.12 mm in diameter, is placed ~0.10 mm from the axis of the parent zone plate, tangent to its edge. This pupil defines the numerical aperture of the objective, 0.0625NA, while the focal distance, 1 mm is defined by the outer zone width of the parent zone plate. A rectangular window next to the off-axis objective zone plate is left uncoated. This window allows transmission of the condenser illumination to the mask at an angle of incidence of 6 degrees. The reflected light from the mask efficiently fills the pupil of the off-axis zone. The off-axis zone plate produces a near-normal image of the mask onto the EUV/SXR sensitive array detector.

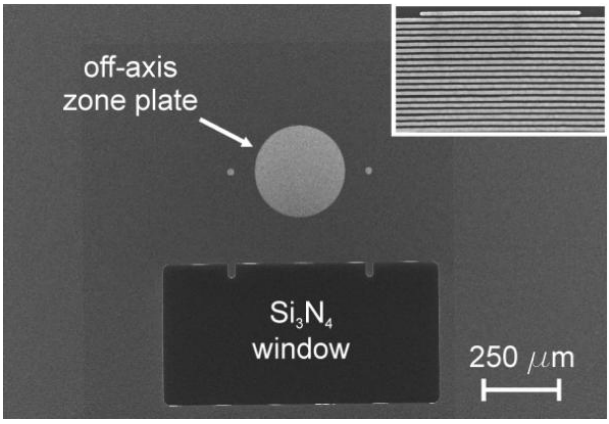

Fig. 3. SEM image of the off-axis zone plate. The Si_3N_4 window provides a path for the illumination from the condenser to reach the EUVL mask. The off axis zone plate produces a near-normal image of the mask onto an EUV sensitive CCD. The insert shows the 40 nm outer zones of the zone plate.

Both zone plates were produced by e-beam lithography on 100 nm thick Si_3N_4 membranes. To increase the efficiency of the microscope the membrane of the objective was further thinned down to 40 nm.

Two samples were available for imaging. One sample consisted of a Mo/Si multilayer coated 500 μm thick Si wafer onto which an absorption test pattern was written. The Mo/Si multilayer was centred at 13.5 nm wavelength to properly simulate an EUVL mask. The sample contained periodic features of different size, from 300 nm half-pitch down to 80 nm half-pitch. Vertical and horizontal 1:1 and 2:1 lines and elbow absorption patterns were available at each half-pitch. The latter are especially useful in characterizing the degree of aberration present in the EUV images since they provide information in two orthogonal directions within the same field-of-view.

The second sample was an EUVL mask from GLOBALFOUNDRIES, Inc. It consisted of a Mo/Si coated, 6×6 in^2, low thermal expansion glass that

contained a series of dark-field and bright-field regions with a variety of test features and extended line patterns. The smallest grating available had a half-pitch of 125 nm.

3 Results

The resolving power of the microscope was evaluated by analyzing the modulation in intensity of EUV images of grating patterns of decreasing half-pitch. Figure 4 shows EUV images of the 140 nm, 120 nm, 100 nm, and 80 nm half-pitch elbow structures along with their respective intensity cross-sections (lineouts). These images were obtained using exposure times of 20 seconds with the laser operating at a repetition rate of 5 Hz. The images have a field of view of ~5×5 μm^2, limited by the size of the illumination beam. They were taken with a magnification of ~610× at which each pixel on the CCD corresponds to 22 nm in the sample plane. This magnification was selected to allow approximately 8 pixels per period in the smallest structures available. The intensity cross-sections, obtained by averaging the intensity of 5 consecutive rows of pixels, were measured for the horizontal and vertical lines. The high modulation obtained for the 80 nm half-pitch structure indicates that the spatial resolution of the system is better than 80 nm.

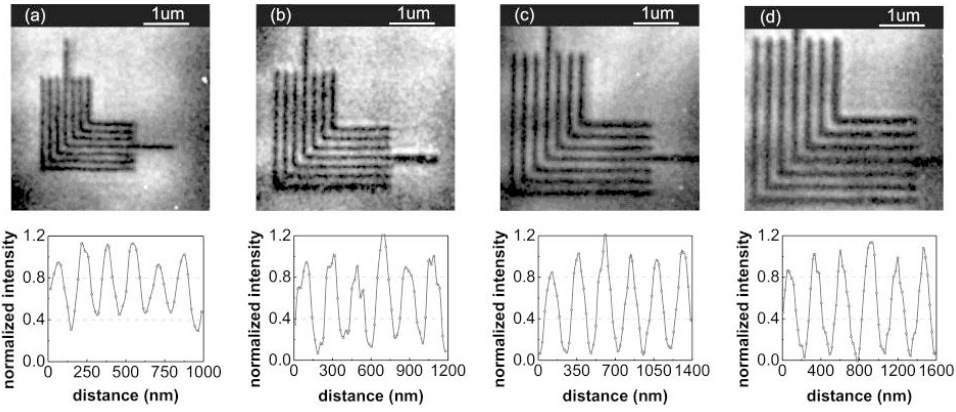

Fig. 4. EUV images and corresponding intensity cross-sections of elbow patterns of 80 nm, 100 nm, 120 nm, and 140 nm half pitch. The high modulation in the intensity cross section of the 880 nm half-pitch elbow indicates that the features are fully resolved.

The Rayleigh resolution of the microscope was independently assessed by analysing the EUV images of Fig. 4 with a correlation method that performs a global assessment of an image and returns a value for the image resolution [15]. The image resolution is obtained from the correlation between a raw SXR image and a series of computer generated templates with decreasing resolution. The templates are constructed by applying different Gaussian filters to a master binary template constructed from the original image. The only required input parameter for the analysis is the microscope's magnification which determines the size of the pixel in the image. To relate the image resolution to the Rayleigh resolution, the method uses a computer generated image of two circular objects separated a distance corresponding to the first minimum of the Airy function as used in the Rayleigh resolution. A value of half-pitch Rayleigh resolution of 53±10 nm was obtained. It is important to point out that this result further assumes incoherent illumination. As it will be shown below, the illumination of the microscope has some degree of coherence.

The Modulation Transfer Function (MTF) of the microscope, which gives a measure of the ability of the microscope for transferring different spatial frequencies, was constructed using the intensity modulation data obtained from the images of Fig. 4 along with the results correlation test. As shown in Fig. 5, the modulation starts to roll off for structures smaller than 120 nm, in agreement with simulations for a 0.0625 NA objective under partially coherent illumination. The dashed line was added to guide the eye.

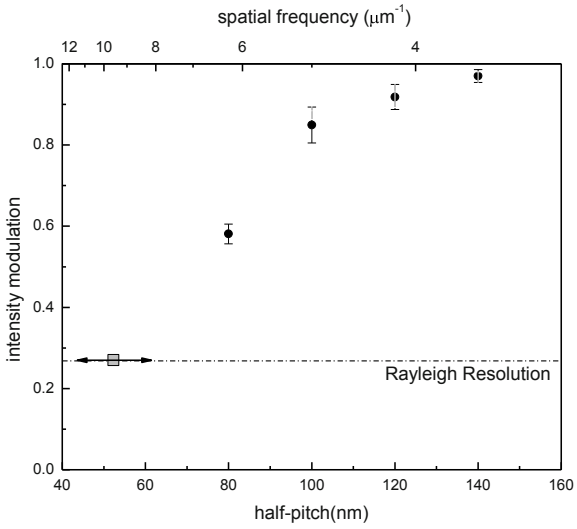

Fig. 5. Modulation Transfer Function for the 13.2 nm wavelength reflection microscope. The MTF was constructed using the line-outs from the images of Fig. 4 (full circles). The results of the correlation method are shown by the square.

The spatial coherence of the microscope was evaluated using a through-focus analysis. For a partially coherent system intensity maxima appear at defocus distances corresponding to the Talbot distances, given by $n \times a^2/\lambda$, where a is the period of the grating; λ, the wavelength of illumination; and n, an integer. Figure 6 shows the intensity modulation for EUV images of a 200 nm half-pitch grating at different defocus distances. The occurrence of secondary maxima indicates that the microscope operates in the partially coherent regime. Comparisons with simulated data using SPLAT [16] indicate that the coherence value, m, of the microscope is approximately 0.25. The coherence parameter can easily be increased to ~0.5, the typical value in an EUVL stepper, by moving the turning mirror (Fig. 1) from shot to shot during image acquisition.

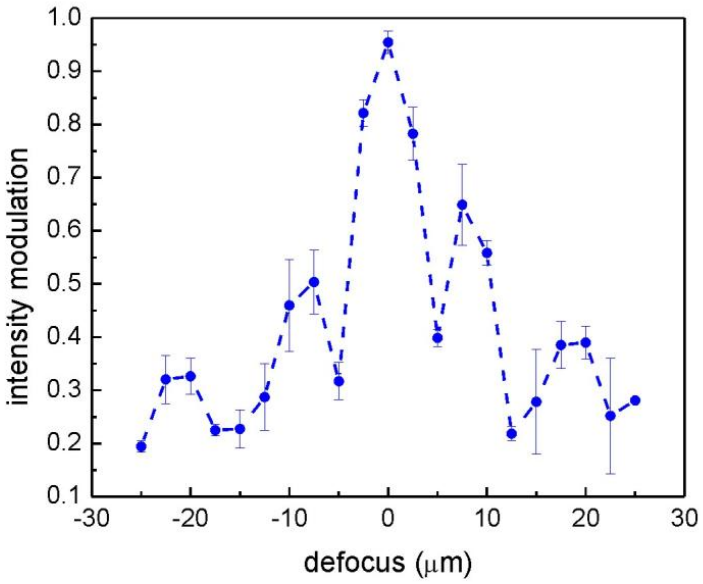

Fig. 6. Intensity modulation versus defocusing distance. The through-focus data indicates that the microscope has a partial coherence parameter, m, of 0.25.

Analysis of the masks print quality requires images, such as those shown in Fig. 7. The images were obtained with an exposure time of 90 seconds with the laser operating at 1 Hz. The condenser was slightly moved from shot to shot during acquisition to increase the illumination uniformity. The images show high illumination uniformity with no discernable aberrations.

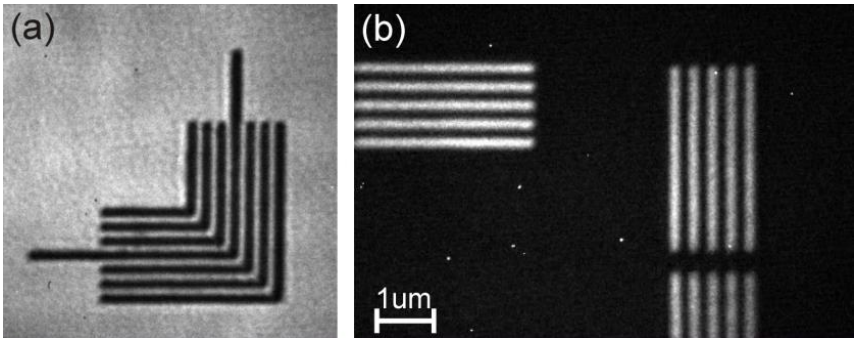

Fig. 7. EUV image of a) a 180 nm half-pitch elbow structure, b) 200 nm half-pitch lines on a GLOBALFOUDRIES mask.

The microscope was used to evaluate the quality of the absorber patterns on the GLOBALFOUNDRIES mask through measurements of line-edge roughness (LER) and normalized image log-slope (NILS). Normalized image log-slope (NILS), measured as the derivative of the logarithm of the image's intensity, assesses the steepness of the intensity slope along the imaged features. Line edge roughness (LER) is a statistical measure of the variation of a feature's edge along the feature's extent and is typically expressed as three times the standard deviation, $3\sigma_{dev}$. Values of LER below 10% of the critical dimension (CD) of the features are considered acceptable. Figure 8 shows the analysis of NILS and LER for a 175 nm half-pitch grating. To obtain these parameters, the image (Fig. 8.a) was normalized in intensity and a threshold value corresponding to the normalized intensity value for which the lines and spaces have a 1:1 ratio was obtained (Fig. 8.b). In this case, the threshold value was ~0.4. A NILS value of 3.58 was obtained by averaging the NILS measured at the intensity threshold for each slope of the average intensity cross-section. LER for each line was measured by evaluating the magnification-corrected location of the occurrence of the intensity threshold for each pixel row of the images (Fig. 8.c). The standard deviation of these values was subsequently calculated for each edge. The measurements were performed across the central 1 μm region of the grating. For the 175 nm half-pitch grating the LER value, 13.55, is below 10% of CD (LER/CD < 0.1).[5]

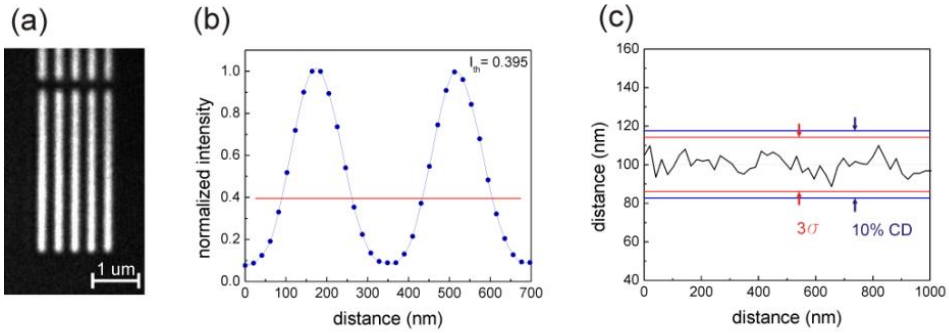

Fig. 8. LER and NILS measurements on 175 nm half-pitch lines

4 Summary

We have demonstrated a compact, actinic aerial image microscope based on EUV/SXR laser illumination capable of obtaining high quality images for the evaluation of EUVL masks. The microscope uses a 13.2 nm wavelength, table-top EUV laser and diffractive optics in a configuration designed to operate under the same illumination condition of a 0.025 NA, 4×-demagnification, EUVL stepper ensuring accurate evaluation of the printability of patterns and defects. The system, can obtain images with a spatial resolution of approximately 55 nm using exposure times of 5 to 90 seconds. Due to the high uniformity and intensity of the illumination, information on key parameters of mask pattern printability such as NILS and LER can readily be obtained from the images. The performance of the microscope, combined with its small footprint make it ideal for mask characterization in industrial settings. Also, the flexible optical design will allow extension to higher numerical apertures as steppers with increasing NA become available. The results presented, and the flexibility of the microscope to extend to smaller technological nodes, opens the path to the realization of practical standalone EUVL metrology tools for HVM.

This work was supported by the Engineering Research Center Program of the National Science Foundation under NSF Award Number EEC-0310717.

5 References

1. C.A. Brewer, F. Brizuela, P. Wachulak, D.H. Martz, W. Chao, E.H. Anderson, D.T. Attwood, A.V. Vinogradov, I.A. Artyukov, A.G.

Ponomareko, V.V. Kondratenko, M.C. Marconi, J.J. Rocca, and C.S. Menonil, *Single-shot extreme ultraviolet laser imaging of nanostructures with wavelength resolution.* Optics Letters, 2008. **33**(5): p. 518-520.

2. P.W. Wachulak, R.A. Bartels, M.C. Marconi, C.S. Menoni, J.J. Rocca, Y. Lu, and B. Parkinson, *Sub 400 nm spatial resolution extreme ultraviolet holography with a table top laser.* Optics Express, 2006. **14**(21): p. 9636-9642.
3. P.W. Wachulak, M.G. Capeluto, M.C. Marconi, C.S. Menoni, and J.J. Rocca, *Patterning of nano-scale arrays by table-top extreme ultraviolet laser interferometric lithography.* Optics Express, 2007. **15**(6): p. 3465-3469.
4. S. Heinbuch, F. Dong, J.J. Rocca, and E.R. Bernstein, *Single photon ionization of hydrogen bonded clusters with a soft x-ray laser: (HCOOH)(x) and (HCOOH)(y)(H2O)(z).* Journal of Chemical Physics, 2007. **126**(24).
5. F. Brizuela, S. Carbajo, A. Sakdinawat, D. Alessi, D.H. Martz, Y. Wang, B. Luther, K.A. Goldberg, I. Mochi, D.T. Attwood, B. La Fontaine, J.J. Rocca, and C.S. Menoni, *Extreme ultraviolet laser-based table-top aerial image metrology of lithographic masks.* Optics Express, 2010. **18**(14): p. 14467-14473.
6. F. Brizuela, G. Vaschenko, C. Brewer, M. Grisham, C.S. Menoni, M.C. Marconi, J.J. Rocca, W. Chao, J.A. Liddle, E.H. Anderson, D.T. Attwood, A.V. Vinogradov, I.A. Artioukov, Y.P. Pershyn, and V.V. Kondratenko, *Reflection mode imaging with nanoscale resolution using a compact extreme ultraviolet laser.* Optics Express, 2005. **13**(11): p. 3983-3988.
7. F. Brizuela, Y. Wang, C.A. Brewer, F. Pedaci, W. Chao, E.H. Anderson, Y. Liu, K.A. Goldberg, P. Naulleau, P. Wachulak, M.C. Marconi, D.T. Attwood, J.J. Rocca, and C.S. Menoni, *Microscopy of extreme ultraviolet lithography masks with 13.2 nm tabletop laser illumination.* Optics Letters, 2009. **34**(3): p. 271-273.
8. G. Vaschenko, C. Brewer, F. Brizuela, Y. Wang, M.A. Larotonda, B.M. Luther, M.C. Marconi, J.J. Rocca, and C.S. Menoni, *Sub-38 nm resolution tabletop microscopy with 13 nm wavelength laser light.* Optics Letters, 2006. **31**(9): p. 1214-1216.
9. A. Barty, Y.W. Liu, E. Gullikson, J.S. Taylor, and O. Wood, *Actinic inspection of multilayer defects on EUV masks*, in *Emerging Lithographic Technologies IX, Pts 1 and 2*, R.S. Mackay, Editor. 2005. p. 651-659.
10. K.A. Goldberg, A. Barty, Y.W. Liu, P. Kearney, Y. Tezuka, T. Terasawa, J.S. Taylor, H.S. Han, and O.R. Wood, *Actinic inspection of extreme ultraviolet programed multilayer defects and cross-*

comparison measurements. Journal of Vacuum Science & Technology B, 2006. **24** (6): p. 2824-2828.

11. K.A. Goldberg, P.P. Naulleau, A. Barty, S.B. Rekawa, C.D. Kemp, R.F. Gunion, F. Salmassi, E.M. Gullikson, E.H. Anderson, and H.S. Han, *Performance of actinic EUVL mask imaging using a zoneplate microscope - art. no. 67305E*, in *Photomask Technology 2007, Pts 1-3*, R.J. Naber, Editor. 2007. p. E7305-E7305.
12. K.A. Goldberg, P. Naulleau, I. Mochi, E.H. Anderson, S.B. Rekawa, C.D. Kemp, R.F. Gunion, H.S. Han, and S. Huh. *Actinic extreme ultraviolet mask inspection beyond 0.25 numerical aperture*. 20082220-2224.
13. J.J. Rocca, Y. Wang, M.A. Larotonda, B.M. Luther, M. Berrill, and D. Alessi, *Saturated 13.2 nm high-repetition-rate laser in nickellike cadmium.* Optics Letters, 2005. **30**(19): p. 2581-2583.
14. D.H. Martz, D. Alessi, B.M. Luther, Y. Wang, D. Kemp, M. Berrill, and J.J. Rocca, *High-energy 13.9 nm table-top soft-x-ray laser at 2.5 Hz repetition rate excited by a slab-pumped Ti:sapphire laser.* Optics Letters. **35**(10): p. 1632-1634.
15. P.W. Wachulak, C.A. Brewer, F. Brizuela, C.S. Menoni, W. Chao, E.H. Anderson, R.A. Bartels, J.J. Rocca, and M.C. Marconi. *Analysis of extreme ultraviolet microscopy images of patterned nanostructures based on a correlation method*. 2008B20-B26.
16. *SPLAT*. -Available from: http://cuervo2.eecs.berkeley.edu/.